Final Technical Report for DE-SC0006681

Project Title: Development of new and integrated isotope tools for characterizing nitrogen-uranium cycling in subsurface environments

PI: David Johnston

Report Title: Constraining the role of iron in environmental nitrogen transformations: Dual stable isotope systematics of abiotic NO_2^- reduction by Fe(II) and its production of N_2O

Report Authors:

Scott D. Wankel[1], Carolyn Buchwald[1], Colleen M. Hansel[1] and David Johnston[2]

1. Department of Marine Chemistry and Geochemistry, Woods Hole Oceanographic Institution, Woods Hole, MA
2. Department of Earth and Planetary Sciences, Harvard University, Cambridge, MA

ABSTRACT

Despite mounting evidence for biogeochemical interactions between iron and nitrogen, our understanding of their environmental importance remains limited. Here we present an investigation of abiotic nitrite (NO_2^-) reduction by Fe(II) or 'chemodenitrification,' and its relevance to the production of nitrous oxide (N_2O), specifically focusing on dual (N and O) isotope systematics under a variety of environmentally relevant conditions. We observe a range of kinetic isotope effects that are regulated by reaction rates, with faster rates at higher pH (~8), higher concentrations of Fe(II) and in the presence of mineral surfaces. A clear non-linear relationship between rate constant and kinetic isotope effects of NO_2^- reduction was evident (with larger isotope effects at slower rates) and is interpreted as reflecting the dynamics of Fe(II)-N reaction intermediates. N and O isotopic composition of product N_2O also suggests a complex network of parallel and/or competing pathways. Our findings suggest that NO_2^- reduction by Fe(II) may represent an important abiotic source of environmental N_2O, especially in iron-rich environments experiencing dynamic redox variations. This study provides a multi-compound, multi-isotope framework for evaluating the environmental occurrence of abiotic NO_2^- reduction and N_2O formation, helping future studies constrain the relative roles of abiotic and biological N_2O production pathways.

INTRODUCTION

Evidence is mounting for the environmental importance of interactions between iron (Fe) and nitrogen (N) in biogeochemistry. For example, the reduction of Fe(III) coupled to the oxidation of ammonium ('feammox') has been recently demonstrated in soils [1-3], while the reduction of nitrate or nitrite coupled to the oxidation of Fe(II) – or chemodenitrification – has been demonstrated across studies of both soils and bacterial cultures and/or enrichments [4-9]. Despite the potential importance of these processes in the fate of nitrogen, our understanding of their significance remains limited. In particular, a number of these reactions may be catalyzed both chemically and biologically and the resulting nitrogenous products vary widely, including ammonium (NH_4^+), nitric oxide (NO), nitrous oxide (N_2O) and dinitrogen (N_2). The relative contribution of these reaction pathways, therefore, has wide implications for ecosystem function (e.g., N retention/loss) and production of potent greenhouse gases. Furthermore, distinguising between biologically and chemically catalyzed pathways has important implications for geobiology, including an improved understanding of the evolution of iron and nitrogen based metabolic systems and a mechanistic understanding of biologically mediated transformations of nitrogen, iron and carbon across a host of modern and historical environments [10].

Natural abundance isotopes of nitrogen and oxygen have proven useful as tools for disentanglng complex networks of environmental nitrogen transformations [11]. In large part, these efforts rely on information gained from environmental samples and/or from experimental cultures grown under environmentally relevant conditions aimed at carefully constraining kinetic isotope effects ($^{15}\varepsilon$ and $^{18}\varepsilon$, for N and O, respectively), as well as establishing the nature of coupling between isotope effects ($^{18}\varepsilon$:$^{15}\varepsilon$). Nevertheless, there remain important gaps in our understanding, in particular with respect to important isotope effects involving key nitrogen

intermediates including nitrite (NO_2^-), nitric oxide (NO), nitrous oxide (N_2O), and hydroxylamine (NH_2OH). For example, although the dual isotope systematics for biologically mediated oxidative processes involving NO_2^- have been characterized (e.g., NO_2^- formation by NH_4^+ oxidation [12]) and NO_2^- oxidation to NO_3^- [13], information on the dual isotope systematics of reductive processes involving NO_2^-, whether biological or abiotic, is more limited [14-17].

Specifically, there has been little investigation into the kinetic isotope effects of N and O catalyzed by abiotic chemical reduction of NO_2^- by Fe(II) – or 'chemodenitrification' [17, 18]. These types of reactions may represent an important control on the dual NO_3^- and NO_2^- isotopic composition in reducing environments high in iron but low in organic carbon (e.g., aquifers) as well as in environments experiencing dynamic redox fluctuations (coastal sediments, estuaries, rivers). Moreover, although abiotic reactions are thought to contribute significantly to the production of the potent greenhouse gas N_2O, little is known about the controls on the N and O isotope composition of its production by these pathways, hindering their use in constraining global sources of N_2O. Thus, there is a need for a systematic investigation of N and O isotope effects catalyzed by chemical reactions with Fe before they can be used to constrain biological/abiotic interactions between N and Fe in the environment.

To this end, we investigated the stable N and O isotope dynamics of the abiotic reduction of NO_2^- by Fe(II) under a range of environmentally relevant conditions, including characterization of the yield and isotopic composition of the product N_2O. As more studies suggest a potential for anaerobic (a)biotic nitrogen transformations coupled with iron cycling, the N and O isotope effects determined here will aid in the application of dual isotopes of nitrite and N_2O for deciphering the underlying biogeochemical mechanisms controlling the fate of N across

a host of environments including aquatic systems, aquifers, soils, sediments and wastewater treatment plants.

MATERIALS AND METHODS

Nitrite reduction experiments

Batch experiments were conducted anaerobically under reaction conditions outlined in Table S1 with 200 μM nitrite and aqueous Fe(II) ranging from 0.5-8.9 mM in the presence and absence of goethite at room temperature. Experiments varied three primary parameters: Fe(II) concentration, solution pH, and the presence/absence of the iron-oxide goethite. All experiments were initiated in anoxic HEPES buffer (30mM) adjusted to the desired pH using NaOH. 140 mL of buffer was added to 160 mL serum bottles and purged with N_2 gas for 30 minutes to remove any trace oxygen. Bottles were then transferred into an anaerobic glove box (5% H_2/ 95% N_2), where Fe(II) was added from a concentrated anoxic $FeCl_2$ stock solution (~1M). Bottles were then pre-incubated by shaking for 3 days and any Fe precipitates were removed by filtration. In a subset of bottles, the Fe(III) oxyhydroxide goethite (FeOOH) (as synthesized and fully characterized previously – see [19]) was added to a final concentration of 250 μM Fe (in bottles with 1mM Fe(II)) and 1mM Fe (in bottles with 5 or 9mM Fe(II)). Following nitrite addition, bottles were sampled ~4 times within the first 6 hours and less frequently thereafter. Between sampling time points, the crimp-sealed bottles were incubated on an orbital shaker at 150 rpm. Samples were measured for Fe(II) and nitrite concentration using standard spectrophotometric methods (see Supplemental Materials). Subsamples were also measured for nitrite N and O isotopes as described below. Finally, 5ml samples of headspace gas composition were taken at

104 the end of the experiment and injected into pre-evacuated headspace vials (20 ml) for N_2O
105 concentration and isotopic composition analysis.

106 In addition to these batch incubations, a subset of these conditions was also run as a
107 parallel 'N_2O time-series' experiment (pH 8, no mineral addition, Fe(II) 1, 5 and 9mM), in which
108 headspace N_2O measurements were made over time using the autosampler of the IRMS system.
109 For each condition, ten 20ml headspace vials were loaded with solutions as described above and
110 placed immediately onto the headspace purge and trap system coupled to the IRMS. The amount
111 and N and O isotopic composition of evolving N_2O was monitored over time.

112

113 **Isotopic Analyses**

114 Nitrogen and oxygen isotope ratios of nitrite (where $\delta^{15}N = [(^{15}R_{sample}/^{15}R_{Air})-1)*1000$ in
115 units of ‰, and $^{15}R = {}^{15}N/{}^{14}N$ and where $\delta^{18}O = [(^{18}R_{sample}/^{18}R_{VSMOW})-1)*1000$ in units of ‰,
116 and $^{18}R = {}^{18}O/{}^{16}O$) samples were measured by chemically converting 20 to 40 nmoles of NO_2^- to
117 N_2O using the azide method in 20ml headspace vials [20]. The evolved N_2O was purified and
118 collected on a modified TraceGas (IsoPrime, Inc.) purge and trap coupled with a Gilson
119 autosampler before isotopic analysis on an isotope ratio mass spectrometer (IsoPrime 100,
120 Elementar Inc.). Internal nitrite isotope standards (WILIS 10, 11 and 20) were run in parallel at 3
121 different sizes to correct for any variations in sample size and instrumental drift. Based on
122 calibrations against isotope standards USGS 32, 34 and 35 for $\delta^{15}N$ [21] and N23, N7373, and
123 N10129 for $\delta^{18}O$ [22], the values of internal standards WILIS 10, 11, and 20 are -1.7, +57.1, and -
124 7.8‰ for $\delta^{15}N$ and +13.2, +8.6 and +47.6‰ for $\delta^{18}O$, respectively. All isotopic values are
125 reported against the VSMOW (for $\delta^{18}O$) or Air (for $\delta^{15}N$) reference scales. Typical
126 reproducibility for $\delta^{15}N$ is ±0.2‰ and for $\delta^{18}O$ is ±0.2‰.

Headspace N_2O isotopic composition was measured in duplicate by direct comparison against the N_2O reference tank on the IRMS system. The composition of this tank ($\delta^{15}N^{bulk}$ = -0.7‰; $\delta^{18}O$ = +39.1‰; site preference (SP) = -5.3‰, where SP = $\delta^{15}N(\alpha) - \delta^{15}N(\beta)$ and α and β refer to the central and outer N atoms in the linear N_2O molecule, respectively) was calibrated directly against aliquots of two previously calibrated N_2O tanks from the Ostrom Lab at Michigan State University. The molar amount of N_2O in the headspace of each experimental bottle was calculated using the linear relationship between IRMS peak area at m/z 44 and injections of known amounts of N_2O (derived from azide conversion of NO_2^-). Reported values have been corrected for any size linearity of isotopic ratios (31/30, 45/44 and 46/44) by using a series of reference tank subsamples injected into 20ml headspace vials using a gastight syringe. Precision for replicate analyses of our reference gas analyzed as samples for $\delta^{15}N$ is ± 0.3‰, for $\delta^{18}O$ is ±0.4‰ and for SP is ±0.8‰.

Mineral Analysis

The speciation of Fe was determined using synchrotron-based X-ray absorption spectroscopy (XAS) [23] (see Supporting Information).

RESULTS AND DISCUSSION

Coupled Nitrite Reduction and Iron Oxidation

Reaction between ferrous Fe and nitrite led to complete removal of 200 μM nitrite under a range of geochemical conditions that varied in initial Fe(II) levels (~0.5-9 mM), pH (7, 8), and in the presence or absence of the mineral sorbent goethite (Figure 1). These findings are

150 consistent with previous studies demonstrating the ability of Fe(II) to chemically reduce nitrite
151 over a large range of experimental conditions [6, 24-26]. Specifically, rapid reaction between high
152 levels of nitrite (~2-43 mM) and ferrous Fe (~5-43 mM) has been documented over a wide pH
153 range (4 to 8) [17, 26-29].

154 Despite complete loss of nitrite, production of ammonium was never observed and thus
155 nitrite was converted to gaseous products in all cases. Indeed, we observed production of N_2O in
156 all experiments (see below); yet, not enough to account for all of the reduced NO_2^- likely
157 pointing to N_2 as an additional product under our experimental pH range. As such, the primary
158 net reactions operative in our experiments are represented by the following equations:

159

160 $$4\,Fe^{2+} + 2NO_2^- + 5H_2O \rightarrow 4\,FeOOH + N_2O_{(g)} + 6H^+ \qquad [1]$$

$$3\,Fe^{2+} + NO_2^- + 4H_2O \rightarrow 3\,FeOOH + \frac{1}{2}N_{2(g)} + 5H^+ \qquad [2]$$

161

162 In comparison to changes in NO_2^-, only a small percentage of dissolved Fe (II) was
163 removed by Fe(II) oxidation in the majority of incubations (Figure S1). Assuming the
164 stoichiometries of reactions R1 and R2, Fe(II) was always well in excess of nitrite in our
165 experiments. An exception to this was the pH 8 experiment conducted at lower Fe(II) ≤1mM,
166 where Fe(II) was completely oxidized over 100 hours, along with the full removal of nitrite.
167 Consistent with the above reactions, the oxidation of Fe(II) led to rapid Fe(III) precipitation in all
168 conditions except for the lowest initial Fe(II) level (0.5 mM) at pH 7. EXAFS spectral analyses
169 (Figure S2) identified these minerals as goethite, ferrihydrite, and magnetite, which were present
170 at varying proportions depending on conditions (Figure S3). At pH 7, dominant phases were
171 goethite and magnetite with relative contribution of magnetite increasing at higher Fe(II) (Figure

S3a). This trend was inversed at higher pH (pH 8), with goethite and ferrihydrite increasing as Fe(II) increased. Interestingly, incubations conducted with exogenous goethite added initially led to the inhibition of magnetite formation under similar initial Fe(II) levels (Figure S3b). Ferrihydrite and goethite were also identified as secondary products in similar batch incubations but with higher nitrite and aqueous Fe(II) levels at pH 7 [17]. In contrast to our findings, however, Jones and colleagues [17] did not observe formation of magnetite, and instead found precipitation of lepidocrocite particularly when nitrite was provided in excess of the initial aqueous Fe(II) concentration. This variability in precipitation patterns is most likely due to differences in the geochemical conditions of the incubations. In particular, when comparing pH 7 incubations the initial aqueous Fe(II) to nitrite ratio in our incubations ranged from 3 to 44 in contrast to a ratio of 0.13 to 4 in Jones et al (2015). These lower ratios are primarily due to the considerably lower nitrite concentrations used in our incubations (200 μM versus 2.5-40 mM), leading to lower rates of reaction and likely allowing for more extensive Fe(II)-induced ripening and conversion of ferrihydrite to magnetite.

Indeed, the rate of aqueous Fe(II) loss and corresponding nitrite reduction varied as a function of pH, initial aqueous Fe(II) concentration, and exogenous goethite addition (Figure 2, Table S2). Initial reduction of nitrite by Fe(II) was linear with initial rates varying from 0.1 to 50 μM h^{-1} at pH 7 and 5.9 to 160 μM h^{-1} at pH 8. Corresponding Fe(II) loss, a combination of both oxidation by nitrite and sorption/precipitation, exhibited initial rates ranging from 1 to 343 μM h^{-1} at pH 7 and 11 to 2300 μM h^{-1} at pH 8 (see Figure S1). Our observed nitrite reduction and Fe(II) loss rates at pH 7 are generally comparable with previous studies using similar reaction conditions (e.g., [28, 30, 31]), while lower than those rates documented at higher nitrite and Fe(II) levels (albeit at lower Fe(II):NO_2^-; [17, 26]). For the 4 different scenarios employed here (pH 7 and

195 8, with/without goethite; Table S1), we observed a linear relationship between Fe(II)
196 concentration and the first order rate constant (hr^{-1}) (Figure 2; Table S2), highlighting the role of
197 Fe(II) concentrations in regulating nitrite reduction rates.

198 Addition of goethite consistently led to higher reaction rates between Fe(II) and nitrite at
199 both pH values and regardless of initial Fe(II) concentration (Figure 2; Table S2). Multiple
200 studies have shown that the presence Fe(III) oxyhydroxides and the sorption of Fe(II) to mineral
201 surfaces or ligands increases rates of nitrite reduction by Fe(II), including reactions with 2-line
202 ferrihydrite, goethite, biogenic magnetite, lepidocrocite, green rust (GR), siderite and wüstite [5, 28,
203 30-34]. These studies consistently indicate faster kinetics for heterogeneous than homogenous
204 Fe(II)-nitrite reactions.

205 For the homogenous reaction conditions between aqueous Fe(II) and nitrite (absence of
206 exogenous goethite), heterogeneous reactions likely also contributed to the observed reaction
207 rates. The rapid formation of Fe(III) minerals upon Fe(II) and nitrite reaction provided a
208 secondary and presumably faster nitrite reduction pathway. Thus, heterogeneous reactions would
209 also be operative with ferrous Fe bound within magnetite (Figure S3) and/or Fe(II) adsorbed onto
210 the secondary precipitates goethite and ferrihydrite.

211

212 ***Nitrite Isotope Systematics***

213 The N and O stable isotope systematics of abiotic nitrite reduction can potentially be
214 useful for distinguishing among nitrite reduction mechanisms in the environment. Here, the $\delta^{15}N$
215 and $\delta^{18}O$ of the remaining nitrite increased during the reaction in all incubations, reflecting
216 positive isotope effects for both N and O during nitrite reduction (Figure 3). Using a closed
217 system Rayleigh model, the ^{15}N isotope effect for nitrite reduction by Fe(II) (hereafter, $^{15}\varepsilon_{NIR}$

ranged from 6‰ to 45‰, while the ^{18}O isotope effect (hereafter, $^{18}\varepsilon_{NIR}$) ranged between 6‰ and 33‰ (Table 1). The ratio of $^{15}\varepsilon_{NIR}$:$^{18}\varepsilon_{NIR}$, was often lower than 1 (Table 1, Figure S4), reflecting a smaller isotope effect for oxygen compared to nitrogen. Oxygen isotopes of nitrite may also readily equilibrate with water as a function of pH and temperature, with faster equilibration occurring at lower pH and higher temperatures [22]. It is therefore possible that the observed oxygen isotope effect of NO_2^- reduction was influenced by oxygen isotope equilibration with water. No difference in $^{15}\varepsilon_{NIR}$:$^{18}\varepsilon_{NIR}$ was observed between experiments at pH 7 and pH 8, suggesting perhaps this factor was not important in our experiments (Table 1). However, given the rapid consumption rates of our relatively small levels of NO_2^- it is also possible that our experiments were unable to catch the influence of this effect. Although, we would not predict high rates of oxygen exchange at pH 8, the very high $\delta^{18}O$ values under high extents of NO_2^- consumption would be particularly sensitive to even a small amount of isotopic exchange and may contribute to slightly lower observed $^{18}\varepsilon_{NIR}$ relative to that of $^{15}\varepsilon_{NIR}$.

Although very little NO_2^- isotope data exist for chemical reduction, our data exhibit a wider range of $^{15}\varepsilon_{NIR}$ and $^{18}\varepsilon_{NIR}$ values than other recent studies (e.g., [17, 35]). While $^{15}\varepsilon_{NIR}$ and $^{18}\varepsilon_{NIR}$ varied from 6 to 45‰ (Table 1) in our experiments, these values were consistent and reproducible under similar experimental conditions. Indeed, differences in the isotope effects correlate well with factors that directly influence reaction rate, including substrate concentration, pH and interactions with minerals (Figure 3, Table 1). In particular, variations in nitrite isotopic fractionation were inversely related to the reaction rate, with higher rates producing lower $^{15}\varepsilon$ values (Figure 4).

In our experiments differences in isotope effects between heterogeneous and homogenous reactions could not be explicitly addressed since even our 'homogenous' reactions exhibited

rapid mineral formation (Figures S2-S3), promoting heterogeneous surface reactions. Even at the lowest levels of mineral precipitation (pH 7) rates were also slower and it is therefore unclear whether the lower isotope effect stemmed from lower overall reaction rate or from reduced interaction with surface-bound Fe(II). If we assume that the rapid reactions were mostly catalyzed by interactions with surface associated Fe(II) and that the slower reactions were less influenced by surface-bound Fe(II), then it is possible that the heterogeneous reaction exhibits a smaller isotope effect for this process, leading to the lower observed net isotope effects at high reaction rates. Future studies should aim to tease apart the relative influence of rate versus mechanism in order to better understand the reaction mechanism.

The observed kinetic isotope effects in the reacting NO_2^- pool are governed by the combination of chemical reactions (e.g., bond forming/breaking) occurring during nitrite reduction. As such, changes in the relative proportions of different mechanisms/pathways (including back reactions) can change the observed isotope effects of the NO_2^- (and other N bearing intermediate) pools. While the net reaction results in the reduction of NO_2^- to N_2O (and and/or N_2 (reactions [1] and [2] above)), the reaction proceeds through one or more nitrogenous and likely Fe-bound nitrogen species (e.g., nitrosyl ($Fe(NO)^+$ or dinitrosyl ($Fe(NO)_2^{2+}$) intermediates, which may have limited stability under these reaction conditions [5, 36-38]. Specifically, we consider the involvement of an Fe(II) intermediate and isotope fractionation occurring at each of the reaction steps given below (reaction 3-5): the reduction of NO_2^- to NO [1], the complexation of NO with Fe(II) [4] and the reduction of the Fe-NO complex to N_2O (or N_2) [5].

$$k_3 \quad Fe^{2+} + NO_2^- + 2H^+ \rightarrow Fe^{3+} + NO_{aq} + H_2O \qquad [3]$$

k_4 $Fe^{2+} + NO_{aq} \rightarrow (Fe(II)\text{-}NO)^{2+}$ [4]

k_5 $(Fe(II)\text{-}NO)^{2+} + H^+ \rightarrow Fe^{3+} + \frac{1}{2}N_2O + \frac{1}{2}H_2O$ [5]

While the forward reactions resulting in the formation of NO (k_3 in R3) or the formation of a nitrosyl complex (k_4 in R4) may occur with a particular isotope effect, the backward reactions (k_{-3} or k_{-4}) may occur with distinctively different isotope effects. Indeed, recent evidence indicates that the initial reduction of NO_2^- to NO (R3) may largely be controlled by an equilibrium reaction [26], in which case the forward/backward reactions give rise to an equilibrium isotope effect. Additionally, NO_2^- $\delta^{18}O$ could be significantly affected by the incorporation of a 'new' O atom (from H_2O) during the reverse reaction [3] in the reverse direction. The influence of this type of pathway reversibility on isotope dynamics has been well documented in the sulfate reduction system [39-43]. Thus, we suggest that the relative ratio of forward to backward reactions plays the key role in regulating our observed isotope effects in the reactant NO_2^- pool. Also, to the degree that the net reaction is multi-step and/or proceeds through multiple (and likely transient) intermediate species and/or through parallel pathways (e.g., reaction R8a vs. R8b), changes in the relative rates of each step will contribute to changes in the net isotope effect observed in the NO_2^- and product N_2O pools.

$Fe(II) + NO_2^- + H_2O \rightarrow FeOOH + NO + H^+$ [6]

$Fe(II) + NO + 2H_2O \rightarrow NO^- + FeOOH + 3H^+$ [7]

$2NO^- + 2H^+ \rightarrow N_2O + H_2O$ [8a]

$2NO^- + 4H^+ \rightarrow N_2 + 2H_2O$ [8b]

283 Likely, all of these factors contribute to our observed relationship between the kinetic
284 isotope effect and reaction rate (Figure 4).
285
286 **Relationship between NO_2^- reduction and N_2O isotope dynamics**
287 The final amount and N and O isotopic composition of the N_2O accumulated in the batch
288 experiment bottles were measured, including the intramolecular nitrogen isotopic composition,
289 or site preference (SP). Complementary to these end product measurements, N_2O formation and
290 isotopic composition was also monitored over time for a subset of these conditions (pH 8, no
291 goethite, and starting Fe(II) concentrations of 0.9, 4.7 and 9.1mM). The endpoint composition of
292 the N_2O in these 'time series' experiments (Figure S5) was consistent with the endpoint
293 measurements of the batch experiment bottles (Figure S6). In general, lower amounts of N_2O
294 accumulated under conditions promoting slower rates of nitrite reduction (not shown). Molar
295 yields of N_2O (e.g., the percentage of NO_2^- converted to N_2O) ranged from ~11 to 52%,
296 reflecting considerable variation in the relative magnitudes of reaction mechanisms involved in
297 chemodenitrification. N and O isotopic composition of the final N_2O ranged from -19.8 to -3.0‰
298 for $\delta^{15}N_{N2Obulk}$ and from +29.3 to +46.4‰ for $\delta^{18}O_{N2O}$ and were strongly correlated, with all but
299 one outlier clustering between -7.4 to -3.0‰ and +38.4 to +46.4‰, respectively (Figure S6). The
300 single outlier N_2O composition corresponds to the only case in which nitrite reduction was not
301 complete, reflecting N_2O produced from only a partially reduced pool of NO_2^-.
302 Comparison of the starting composition of the reactant NO_2^- with the product N_2O offers
303 important insights into reaction mechanisms. The elevated $\delta^{18}O_{N2O}$ values relative to NO_2^-,
304 relative to the starting NO_2^-, reflect the influence of branching effects by the preferential removal
305 of ^{16}O during reduction steps of both NO_2^- and NO ^{16}. Together with the strong correlation

306 between the $\delta^{15}N$ and $\delta^{18}O$ of product N_2O (Figure S6) this indicates a strong coupling of the
307 kinetic isotope effect on N and the combined kinetic and branching isotope effects on oxygen
308 during the formation of N_2O. The final $\delta^{15}N$ of the accumulated N_2O was on average ~8‰ lower
309 than the $\delta^{15}N$ of the starting NO_2^-, with higher N_2O yields exhibiting smaller differences
310 (excluding the case in which NO_2^- did not fully react – Figure 1).

311 As all of the reacted NO_2^- was not accounted for in the product N_2O, another N-bearing
312 pool must represent the mass balance complement to the N_2O pool, having a higher $\delta^{15}N$ than the
313 starting NO_2^-. Initial product N_2O $\delta^{15}N$ values during the time series experiments were lower
314 than the N isotope effects calculated from the NO_2^- pool (Figure S5) reflecting production of a
315 separate N bearing pool. At high N_2O yields (~30-50%), end point $\delta^{15}N$ values were on average
316 ~4 to 8‰ lower than starting NO_2^- $\delta^{15}N$ values – and by mass balance imply production of an N-
317 bearing pool at least several permil higher than the starting NO_2^- $\delta^{15}N$ values. Jones and others [17]
318 observed similar results, suggesting that isotopically heavier N must have accumulated in the NO
319 pool. Under similar reaction conditions (e.g. pH 7, very high NO_2^- and Fe(II)), Kampschreur and
320 colleagues [26] observed complete recovery of NO_2^- as NO and N_2O – suggesting that the missing
321 mass balance complement to the N_2O is likely to be found as NO. Under the higher pH
322 conditions of our time series experiment (pH 8), however, NO was only observed at low levels
323 (qualitatively observed as separate peaks while monitoring masses 30 and 31 on the IRMS
324 during N_2O analyses) and only under low Fe(II) conditions (0.9mM) suggesting that, while
325 possibly an important transient intermediate, gas phase NO did not appear to have been a
326 significant end product (< ~5%). A lack of observed NO accumulation under our higher Fe(II)
327 conditions also appears to highlight the role of Fe(II) in providing the forward kinetic drive
328 (and/or complexation of NO) and likely promoting formation of Fe-bound nitrosyl species (as in

329 reaction R4 above). In comparing the likelihood of an NO vs N_2 pool as the missing mass
330 balance complement of the low $\delta^{15}N$ N_2O, Jones and others (2015) suggested an NO product
331 pool having a higher $\delta^{15}N$ as a more parsimonious explanation since it is less reduced than N_2O
332 (making the assumption that an N_2 pool derived from an N_2O precursor should be isotopically
333 lower than the N_2O). However, based on the apparently low observed accumulation of NO in our
334 time series measurements at pH 8, together with the assumption that a high $\delta^{15}N$ N_2 pool
335 deriving from N_2O reduction would be unlikely, we suggest instead that the production of N_2 and
336 N_2O may be occurring in parallel, competing reactions (as in R8a and R8b), under our
337 experimental conditions (with the production of N_2 having a smaller isotope effect than the
338 production of N_2O). Alternatively, some proportion of NO may have remained bound in a
339 nitrosyliron complex under the higher dissolved Fe(II) conditions. Indeed the difference in
340 proportion of end products is related to differences in the formation kinetics and stability of
341 (di)nitrosyl intermediates, which are sensitive to pH [36, 38]. Either way, whether the missing N
342 pool is comprised of NO, as observed and inferred by others [17, 26], or is comprised primarily of
343 N_2 as appears to be the case in our experiments, the N isotopic composition of the N_2O offers a
344 useful perspective on the source of N and the isotope systematics of N_2O release by
345 chemodenitrification.

346 The intramolecular ^{15}N site preference of the product N_2O also reflects differences in the
347 governing reaction mechanisms. N_2O SP values both from the batch experiments and the time
348 series measurements ranged from -0.4 to +26.0‰ with endpoint values correlating with final
349 concentration and yield of N_2O (Figure 5). In our time series experiments, higher levels of Fe(II)
350 lead to more consistently elevated SP values starting ~ +14.5‰ and increasing to ~ +26.0‰
351 (Figure S5) – similar to previous observations of N_2O SP by chemodenitrification falling

between +10 and +22‰ [17]. In contrast, under lower Fe(II) conditions (~0.9mM) initial SP values were as low as 0‰, although eventually increased to 26.0‰ before reaching a final value of 15.2‰ (Figure S5). Compared to $\delta^{15}N_{N2Obulk}$ and $\delta^{18}O_{N2O}$, which reflect the combined influence of both the composition of reactants (e.g., NO_2^-) and the kinetic isotope effects associated with the reaction pathways, SP is thought to be independent of the $\delta^{15}N$ of the N source and instead reflect only formation pathway. Specifically, the combination of two NO precursor molecules to form N_2O in a singly catalyzed reaction should result in very little difference between the $\delta^{15}N$ of the beta (outer) and alpha (inner) N atoms, such as is observed for nitric oxide reductases in denitrifying bacteria [44, 45]. In contrast, mechanisms whereby combination of two NO molecules proceeds via formation of an O-N=N-O intermediate favors breaking of ^{14}N-O bond over a ^{15}N-O bond – and promotes the ^{15}N enrichment of the alpha position (e.g., elevated SP value), as is thought to occur during NH_2OH decomposition and N_2O production by ammonia oxidizing bacteria [46, 47] and denitrifying fungi [48-50]. Elevated SP values (+35‰) have in fact also been observed in chemical reactions involving NH_2OH and NO_2^- including in the presence of Fe catalysts – although the decomposition of NH_2OH may play the primary role rather than NO_2^- [35]. Results of chemical reduction of NO_2^- in experiments using other reductants (e.g., trimethylamine-borane) have also yielded elevated SP values – suggesting an important role for an intermediate species [44]. Studies investigating reduction of NO_2^- by either aqueous Fe(II) or Fe(II)-containing primary minerals have also noted production of N_2O having positive SP values up to 22‰ [17, 51], although low SP values have also been reported [18]. We suggest that the range of SP values observed in field studies [51] and in lab studies such as ours and those of others [17, 18], reflects shifts in the balance of at least two mechanisms of N_2O formation and specifically the relative involvement of intermediate nitrosyl and dinitrosyl species (and the factors regulating

their formation and stability; [5, 36, 38]). Indeed, in our experiments, higher N_2O yields correspond with higher reduction rates and in turn higher concentrations of Fe(II). Thus, in summary, the high Fe(II) conditions of our experiments apparently favor the formation of nitrosyl-iron complexes as reaction intermediates and precursors for reactions yielding elevated SP values for product N_2O. On the other hand, lower levels of Fe(II) and the correspondingly slower reduction of NO_2^- apparently produce N_2O having generally lower SP values (Figure 5; Figure S5).

Environmental Implications

Here we have shown that abiotic reduction of nitrite by Fe(II) is rapid at environmentally relevant pH and Fe(II) concentrations. Indeed, we demonstrate that factors regulating the rates of this chemical process in the environment include reactant concentrations, surface interactions and pH. Further, these factors appear to control the relative proportions of reaction pathways, with strong implications for the isotopic evolution of reactant NO_2^- as well as the isotopic composition and yield of product N_2O. Specifically, even though elevated levels of Fe(II) increase reaction rate, the homogeneous reaction of NO_2^- with aqueous Fe(II) is kinetically slow under our experimental conditions compared to biological reduction (e.g., [52]). Nevertheless, in most natural environments at circumneutral pH, aqueous Fe(II) is found adsorbed onto mineral surfaces and/or bound as ligands. Thus, while the homogenous reaction of aqueous Fe(II) with NO_2^- may be kinetically inhibited, the heterogeneous reaction will most likely drive environmental chemodenitrification. In fact, our data also demonstrate dramatically increased reactivity of NO_2^- with surface associated Fe(II). In all cases exhibiting Fe-oxide formation, rates of nitrite reduction were dramatically higher (Figure 2) as well as corresponding yields of N_2O. Thus, under redox conditions promoting production of Fe(II) and conditions enabling sorption of

Fe onto mineral surfaces (e.g., soils, porewaters, permeable sediments, riparian zones), the kinetic drive for abiotic NO_2^- reduction by Fe(II) is substantial – as is the potential for its significance as an abiotic source of N_2O to the atmosphere. Notably, recent work with a culture of nitrate-reducing iron oxidizing bacteria also suggests that anaerobic Fe oxidation actually occurs as a chemical side reaction upon the intracellular production of NO_2^- and Fe oxides, raising the possibility that anaerobic Fe oxidation by other nitrate reducing microbes may also stem primarily from chemical interactions rather than direct enzymatic catalysis [5, 53].

The sensitivity of the nitrite isotope effects and the product N_2O to reaction conditions will complicate interpretation of natural abundance isotope values for detecting reactions with Fe(II). Accordingly, environmental studies will need to fully account for factors including pH and Fe(II) concentrations/fluxes, abundance and form of Fe–bearing minerals, and concentrations/fluxes of nitrite. Constraining pH will be especially crucial to account for potential oxygen isotope exchange with water, which is rapid at pH values < 7 [22]. Many of the ecosystems in which nitrite accumulation may be important such as groundwater, estuaries and coastal sediments may also exhibit dynamic changes in pH (during tidal flushing of an estuary, or a storm runoff event, for example). Currently, rates of nitrite-water oxygen isotope equilibration have only been quantified in seawater [54]. Thus, in order to fully exploit NO_2^- oxygen isotopes in other ecosystems, future work on exchange rates across a range of salinity will be necessary.

With this improved understanding of controls on N_2O production by abiotic nitrite reduction, future studies should focus on establishing the importance of chemodenitrification in the environment especially under environmental conditions in which it may outcompete biological nitrite reduction. For example, in environments exhibiting rapidly fluctuating redox

conditions, such as estuarine sediments and permeable coastal and shelf sediments, high fluxes of Fe(II) released by iron-reducing bacteria and/or by abiotic reduction by sulfur intermediates are often closely juxtaposed with elevated nitrogen concentrations in overlying water. Such conditions could represent prime hotspots for abiotic reactions between NO_2^- and Fe(II) and the abiotic formation of N_2O.

426 **Table 1.** Observed N and O isotope effects for abiotic reduction of nitrite by Fe(II). In some
427 cases reactions were too fast for reliable measurement of NO_2^- isotopes. ND = not enough nitrite
428 detected.

429

pH	Starting [Fe(II)] (mM)	**Goethite**	$^{15}\varepsilon$ **(‰)**	$^{18}\varepsilon$ **(‰)**	$^{18}\varepsilon : {}^{15}\varepsilon$
7	0.5	No	33.9±24.8	24.8±15.9	0.7
7	4.7	No	25.1±2.5	18.1±2.1	0.7
7	8.4	No	6.1±1.0	7.8±0.2	1.3
8	0.6	No	22.6±1.0	14.4±1.6	0.6
8	4.2	No	6.6±1.1	5.7±1.3	0.9
8	6.3	No	N.D.	N.D.	N.D.
7	0.8	Yes	44.8±9.7	33.0±8.3	0.7
7	4.8	Yes	11.8±0.6	11.2±0.3	0.9
7	7.9	Yes	5.9	5.2	0.9
8	1.0	Yes	15.1±0.5	11.2±0.6	0.7
8	4.5	Yes	N.D.	N.D.	N.D.
8	8.9	Yes	N.D.	N.D.	N.D.

430

431

ACKNOWLEDGEMENTS

This work was supported in part by National Science Foundation grant EAR-1252161 to SDW and CMH and grant OCE-1260373 to SDW. Early experiments and foundational research for this work were supported by Exploratory Funding from the DOE Office of Subsurface Biogeochemical Research (DOE-Grants-SC0006681). CB was supported in part by a postdoctoral fellowship from the NSF Center for Dark Energy Biosphere Investigations (C-DEBI) and KCG aw supported by a Herchel-Smith Harvard Undergraduate Science Research Fellowship. We would also like to acknowledge Zoe Sandwith and Net Charoenpong for assistance with lab work and isotopic analyses. Finally, the authors also thank Dr. David Johnston for insightful conversation, helpful input and generous support of preliminary experimental work on the nature of interactions between iron and nitrogen cycling.

CONFLICT OF INTEREST

The authors declare no competing conflict of interest.

REFERENCES

1. Li, X.; Hou, L.; Liu, M.; Zheng, Y.; yin, G.; Lin, A.; Xianbao; Cheng, L.; Li, Y.; Hu, X., Evidence of nitrogen loss from anaerobic ammonium oxidation coupled with ferric iron reduction in an intertidal wetland. *Environmental Science & Technology* **2015**.
2. Shrestha, J.; Rich, J. J.; Ehrenfeld, J. G.; Jaffe, P. R., Oxidation of ammonium to nitrite under iron-reducing conditions in wetland soils: Laboratory, field demonstrations, and push-pull rate determination. *Soil Science* **2009,** *174*, (3), 156-164.
3. Yang, W. H.; Weber, K. A.; Silver, W. L., Nitrogen loss from soil through anaerobic ammonium oxidation coupled to iron reduction. *Nature Geoscience* **2012,** *5*, 538-541.
4. Klueglein, N.; Kappler, A., Abiotic oxidation of Fe(II) by reactive nitrogen species in cultures of the nitrate-reducing Fe(II) oxidizer Acidovorax sp BoFeN1 - questioning the existence of enzymatic Fe(II) oxidation. *Geobiology* **2012**.
5. Kopf, S. H.; Henny, C.; Newman, D. K., Ligand-enhanced abiotic iron oxidation and the effects of chemical versus biological iron cycling in anoxic environments. *Environmental Science & Technology* **2013,** *47*, 2602-2611.
6. Picardal, F. W., Abiotic and microbial interactions during anaerobic transformations of Fe(II) and NO_x^-. *Frontiers Microb.* **2012,** *3*, (57), 6.
7. Straub, K.; Benz, M.; Schink, B.; Widdel, F., Anaerobic Nitrate Dependent Microbial Oxidation of Ferrous Iron. *Applied and Environmental Microbiology* **1996,** *62*, (4), 1458-1460.
8. Weber, K. A.; Achenbach, L. A.; Coates, J. D., Microorganisms pumping iron: Anaerobic microbial iron oxidation and reduction. *Nature* **2006,** *4*, 752-764.
9. Melton, E. D.; Swanner, E. D.; Behrens, S.; Schmidt, C.; Kappler, A., The interplay of microbially mediate and abiotic reactions in the biogeochemical Fe cycle. *Nature Reviews in Microbiology* **2014,** *12*, 797-808.
10. Falkowski, P. G.; Scholes, J.; Boyle, E.; Canadell, J.; Canfield, D. E.; Elser, J.; Gruber, N.; Hibbard, K.; Högberg, P.; Linder, S.; MacKenzie, F.; Moore III, B.; Pedersen, T. F.; Rosenthal, Y.; Seitzinger, S. P.; Smetacek, V.; Steffen, W., The Global Carbon Cycle: A Test of Our Knowledge of Earth as a System. *Science* **2001,** *290*, (5490), 291.
11. Kendall, C.; Elliott, E. M.; Wankel, S. D., Tracing anthropogenic inputs of nitrogen to ecosystems. In *Stable isotopes in ecology and environmental science*, 2nd ed.; Michener, R. H.; Lajtha, K., Eds. Blackwell Publishing: 2007; p 592.
12. Casciotti, K. L.; McIlvin, M.; Buchwald, C., Oxygen isotopic exchange and fractionation during bacterial ammonia oxidation. *Limnology and Oceanography* **2010,** *55*, (2), 753-762.
13. Buchwald, C.; Casciotti, K. L., Oxygen isotopic fractionation and exchange during bacterial nitrite oxidation. *Limnology and Oceanography* **2010,** *55*, (3), 1064-1074.

14. Brunner, B.; Contreras, S.; Lehmann, M. F.; Matantseva, O.; Rollog, M.; Kalvelage, T.; Klock, G.; Lavik, G.; Jetten, M. S. M.; Kartal, B.; Kuypers, M. M., Nitrogen isotope effects induced by anammox bacteria. *Proceedings of Ocean Observing '09: Sustained ocean observations and information for society* **2013,** *110*, (47), 18994-18999.
15. Bryan, B.; Shearer, G.; Skeeters, J.; Kohl, D., Variable expression of the nitrogen isotope effect associated with denitrification of nitrite. *Journal of Biological Chemistry* **1983,** *258*, 8613-8617.
16. Casciotti, K. L.; Sigman, D. M.; Galanter-Hastings, M.; Böhlke, J. K.; Hilkert, A., Measurement of the oxygen isotopic composition of nitrate in seawater and freshwater using the denitrifier method. *Analytical Chemistry* **2002,** *74*, 4905-4912.
17. Jones, L. C.; Peters, B.; Lezama Pacheco, J. S.; Casciotti, K. L.; Fendorf, S., Stable isotopes and iron oxide mineral products as markers of chemodenitrification. *Environmental Science & Technology* **2015,** *49*, 3444-3452.
18. Samarkin, V. A.; Madigan, M. T.; Bowles, M. W.; Casciotti, K. L.; Priscu, J. C.; McKay, C. P.; Joye, S. B., Abiotic nitrous oxide emission from the hypersaline Don Juan Pond in Antarctica. *Nature Geoscience* **2010,** *3*, 341-344.
19. Ekstrom, E. B.; Learman, D. R.; Madden, A. S.; Hansel, C. M., Contrasting effects of Al substitution on microbial reduction of Fe(III) (hydr)oxides. *Geochim. Cosmochim. Acta* **2010,** *74*, 7086-7099.
20. McIlvin, M.; Altabet, M. A., Chemical conversion of nitrate and nitrite to nitrous oxide for nitrogen and oxygen isotopic analysis in freshwater and seawater. *Analytical Chemistry* **2005,** *77*, (17), 5589-5595.
21. Böhlke, J.; Mroczkowski, S.; Coplen, T. B., Oxygen isotopes in nitrate: new reference materials for ^{18}O:^{17}O:^{16}O measurements and observations on nitrate-water equilibration. *Rapid Communications in Mass Spectrometry* **2003,** *17*, 1835-1846.
22. Casciotti, K. L.; Böhlke, J. K.; McIlvin, M.; Mroczkowski, S.; Hannon, J., Oxygen isotopes in nitrite: Analysis, calibration and equilibration. *Analytical Chemistry* **2007,** *79*, 2427-2436.
23. Hansel, C. M.; Benner, S. G.; Neiss, J.; Dohnalkova, A. C.; Kukkadapu, R. K.; Fendorf, S., Secondary mineralization pathways induced by dissimilatory iron reduction of ferrihydrite under advective flow *Geochimica et Cosmochimica Acta* **2003,** *67*, (16), 2977-2992.
24. Sorenson, J.; Christensen, D.; Jorgensen, B. B., Volatile fatty acids and hydrogen as substrates for sulfate-reducing bacteria in anaerobic marine sediment. *Appl. Environ. Microb.* **1981,** *42*, 5-11.
25. van Cleemput, O.; Baert, L., Nitrite stability influenced by iron compounds. *Soil Biology & Biochemistry* **1983,** *15*, (2), 137-140.
26. Kampschreur, M. J.; Kleerebezem, R.; de Vet, W. W.; van Loosdrecht, M., Reduced iron induced nitric oxide and nitrous oxide emission. *Water Research* **2011,** *45*, 5945-5952.

27. Moraghan, J. T.; Buresh, R. J., Chemical reduction of nitrite and nitrous oxide by ferrous iron. *Soil Science Society of America Journal* **1977,** *41*, (1), 47-50.
28. Tai, Y.-L.; Dempsey, B. A., Nitrite reduction with hydrous ferric oxide and Fe(II): Stoichiomtery, rate and mechanism. *Water Research* **2009,** *43*, 546-552.
29. Nelson, D.; Bremner, J., Gaseous products of nitrite decomposition in soils. *Soil Biology and Biochemistry* **1970,** *2*, (3), 203-204.
30. Dhakal, P.; Matocha, C. J.; Huggins, F.; Vandiviere, M., Nitrite reactivity with magnetite. *Environmental Science and Technology* **2013,** *47*, 6206-6213.
31. Sorensen, J.; Thorling, L., Stimulation by lepidocrocite (ϒ-FeOOH) of Fe(II)-dependent nitrite reduction. *Geochimica et Cosmochimica Acta* **1991,** *55*, 1289-1294.
32. Coby, A.; Picardal, F. W., Inhibition of NO_3^- and NO_2^- reduction by microbial Fe(III) reduction: Evidence of a reaction between NO_2- and cell surface-bound Fe(II). *Applied and Environmental Microbiology* **2005,** *71*, (9), 5267-5274.
33. Hansen, H. C. B.; Borggaard, O. K.; Sorensen, J., Evaluation of the free energy of formation of Fe(II)-Fe(III) hydroxide-sulphate (green rust) and its reduction of nitrite. *Geochim. Cosmochim. Acta* **1994,** *58*, (12), 2599-2608.
34. Rakshit, S.; Matocha, C. J.; Coyne, M. S., Nitrite reduction by siderite. *Soil Science Society of America Journal* **2007,** *72*, 1070-1077.
35. Heil, J.; Wolf, B.; Brüggeman, N.; Emmenegger, L.; Tuzson, B.; Verecken, H.; Mohn, J., Site-specific ^{15}N isotopic signatures of abiotically produced N_2O. *Geochimica et Cosmochimica Acta* **2015**.
36. Bonner, F. T.; Pearsall, K. A., Aqueous Nitrosyliron(II) Chemistry. I. Reduction of nitrite and nitric oxide by Iron(II) and (Trioxodinitrato)iron(II) in Acetate Buffer. Intermediacy of nitrosyl hydride. *Inorganic Chemistry* **1982,** *21*, (1973-1978).
37. Kustin, K.; Taub, I.; Weinstoc, E., A kinetic study of formation of ferrous-nitric oxide complex. *Inorganic Chemistry* **1966,** *5*, (1079-1082).
38. Pearsall, K. A.; Bonner, F. T., Aqueous Nitrosyliron(II) Chemistry. 2. Kinetics and mechanisms of nitric oxide reduction. The dinitrosyl complex. *Inorganic Chemistry* **1982,** *21*, 1978-1985.
39. Bradley, A. S.; Leavitt, W. D.; Johnston, D. T., Revisiting the dissimilatory sulfate reduction pathway. *Geobiology* **2011,** *9*, (446-457).
40. Brunner, B.; Einsiedl, F.; Arnold, G. L.; Müller, I.; Templer, S.; Bernasconi, S. M., The reversibility of dissimilatory sulphate reduction and the cell-internal multi-step reduction of sulphite to sulphide: Insights from the oxygen isotope composition of sulphate. *Isotopes in Environmental and Health Studies* **2011,** *48*, (1), 33-54.
41. Holler, T.; Wegener, G.; Niemann, H.; Deusner, C.; Ferdelman, T. G.; Boetius, A.; Brunner, B.; Widdel, F., Carbon and sulfur back flux during anaerobic microbial oxidation of methane and coupled sulfate reduction. *Proceedings of Ocean Observing '09: Sustained ocean observations and information for society* **2011,** *108*, (52), E1484-E1490.

42. Rees, C., A steady-state model for sulphur isotope fractionation in bacterial reduction processes. *Geochimica et Cosmochimica Acta* **1973,** *37*, 1141-1162.
43. Wankel, S. D.; Bradley, A. S.; Eldridge, D. L.; Johnston, D. T., Determination and application of the equilibrium oxygen isotope effect between water and sulfite. *Geochimica et Cosmochimica Acta* **2014,** *125*, 694-711.
44. Toyoda, S.; Mutobe, H.; Yamagishi, H.; Yoshida, N.; Tanji, Y., Fractionation of N2O isotopomers during production by denitrifier. *Soil Biology & Biochemistry* **2005,** *37*, (8), 1535-1545.
45. Yamazaki, T.; Hozuki, T.; Arai, K.; Toyoda, S.; Koba, K.; Fujiwara, T.; Yoshida, N., Isotopomeric characterization of nitrous oxide produced by reaction of enzymes extracted from nitrifying and denitrifying bacteria. *Biogeosciences* **2014,** *11*, 2679-2689.
46. Frame, C.; Casciotti, K. L., Biogeochemical controls and isotopic signatures of nitrous oxide production by a marine ammonia-oxidizing bacterium. *Biogeosciences* **2010,** *7*, 2695-2709.
47. Sutka, R. L.; Ostrom, N. E.; Ostrom, P. H.; Gandhi, H.; Breznak, J., Nitrogen isotopmer site preference of N_2O produced by *Nitrosomonas europea* and *Methylococcus capsulatus* Bath. *Rapid Communications in Mass Spectrometry* **2003,** *17*, 738-745.
48. Rohe, L.; Anderson, T.-H.; Braker, G.; Flessa, H.; Giesemann, A.; Lewicka-Szczebak, D.; Wrage-Monig, N.; Well, R., Dual isotope and isotopomer signatures of nitrous oxide from fungal denitrification - a pure culture study. *Rapid Communications in Mass Spectrometry* **2014,** *28*, 1893-1903.
49. Sutka, R. L.; Adams, G.; Ostrom, N. E.; Ostrom, P. H., Isotopologue fractionation during N2O production by fungal denitrification. *Rapid Communications in Mass Spectrometry* **2008,** *22*, 3989-3996.
50. Yang, H.; Gandhi, H.; Ostrom, N. E.; Hegg, E. I., Isotopic fractionation by a fungal P450 Nitric Oxide Reductase during the Production of N2O. *Environmental Science & Technology* **2014,** *48*, 10707-10715.
51. Peters, B.; Casciotti, K. L.; Samarkin, V. A.; Madigan, M. T.; Schutte, C. A.; Joye, S. B., Stable isotope analyses of NO2-, NO3- and N2O in the hypersaline ponds and soils of the McMurdo Dry Valleys, Antarctica. *Geochimica et Cosmochimica Acta* **2014,** *135*, 87-101.
52. Betlach, M. R.; Tiedje, J. M., Kinetic explanation for accumulation of nitrite, nitric oxide and nitrous oxide during bacterial denitrification. *Applied and Environmental Microbiology* **1981,** *42*, (6), 1074-1084.
53. Klueglein, N.; Kappler, A., Abiotic oxidation of Fe(II) by reactive nitrogen species in cultures of the nitrate-reducing Fe(II) oxidizer *Acidovorax* sp. BoFeN1 - questioning the existence of enzymatic Fe(II) oxidation. *Geobiol.* **2013,** *11*, 396.
54. Buchwald, C.; Casciotti, K. L., Isotopic ratios of nitrite as tracers of the sources and age of oceanic nitrite. *Nature Geoscience* **2013,** *6*, 309-313.

608

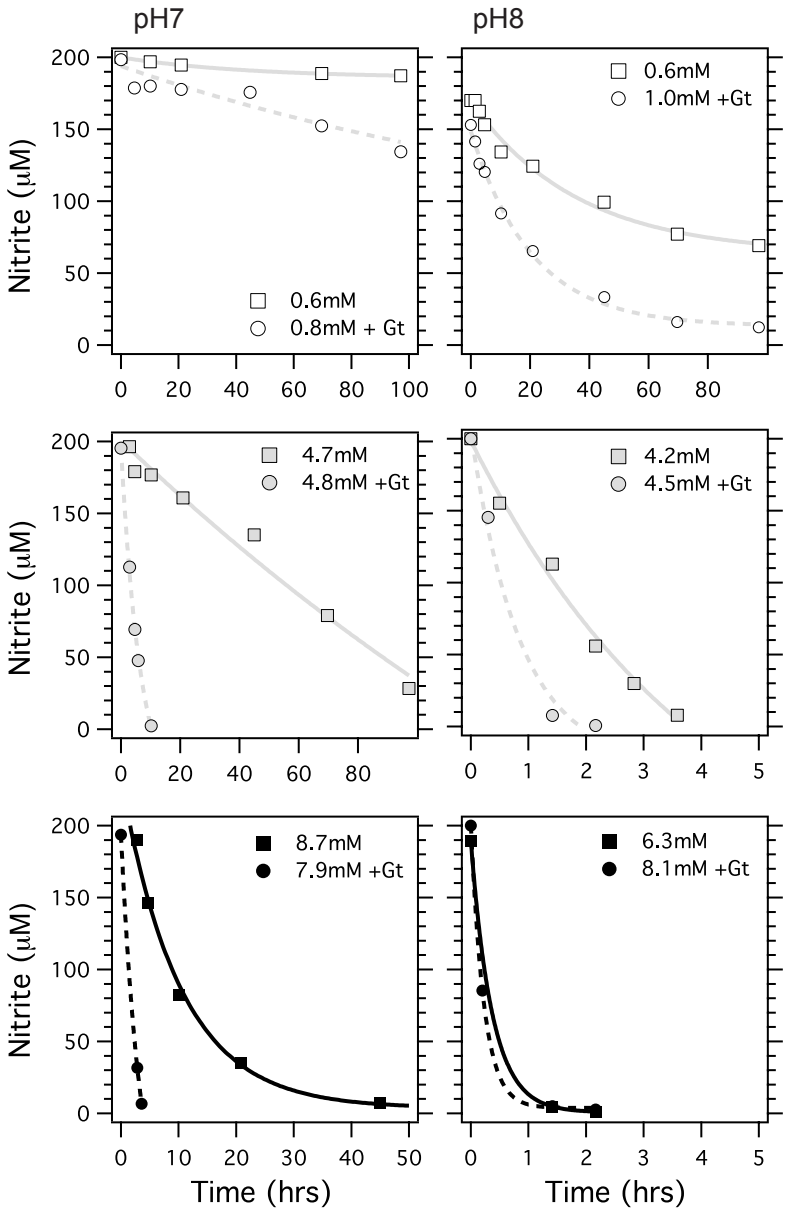

Figure 1. Reaction of nitrite with aqueous Fe(II) as a function of time. Rates of nitrite reduction were faster at higher Fe(II) concentrations, higher pH and in the presence of exogenous goethite. Note the time scale change at higher iron and high pH.

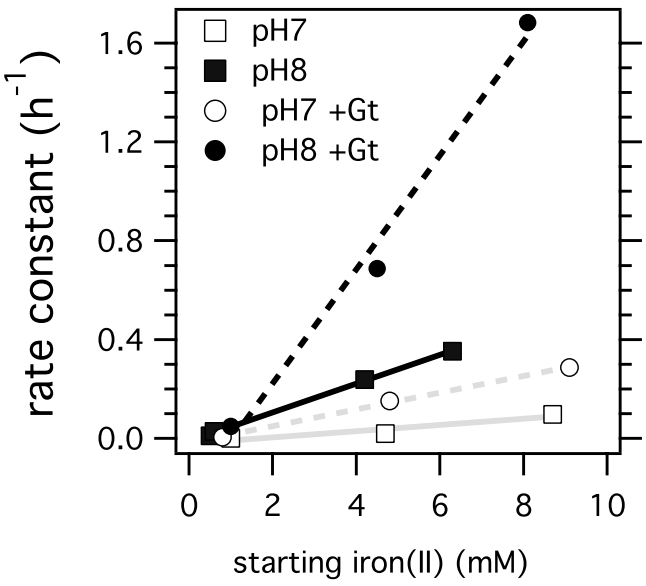

Figure 2. Pseudo-first order rate constants (with respect to NO_2^-) varied linearly with starting Fe(II) concentration, with faster rates at higher pH and in the presence of an FeOOH (goethite) mineral surface. Rate constants were calculated assuming a pseudo-first order rate with Fe(II) in excess of nitrite, and exponential fitting of nitrite concentration over time.

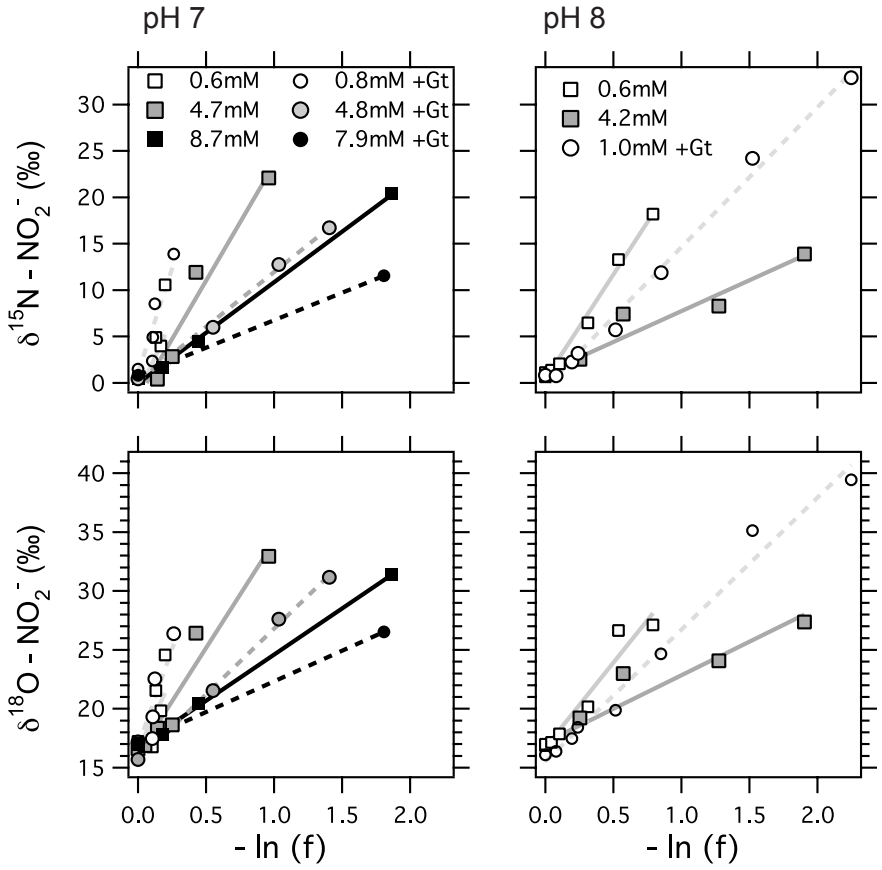

Figure 3. Closed system Rayleigh plots illustrating differences in the observed isotope effects of nitrite reduction by Fe(II) for δ^{15}N-NO_2 (top) and δ^{18}O-NO_2 (bottom) at pH 7 (right) and pH 8 (left). Dotted lines indicate experiments containing amended goethite.

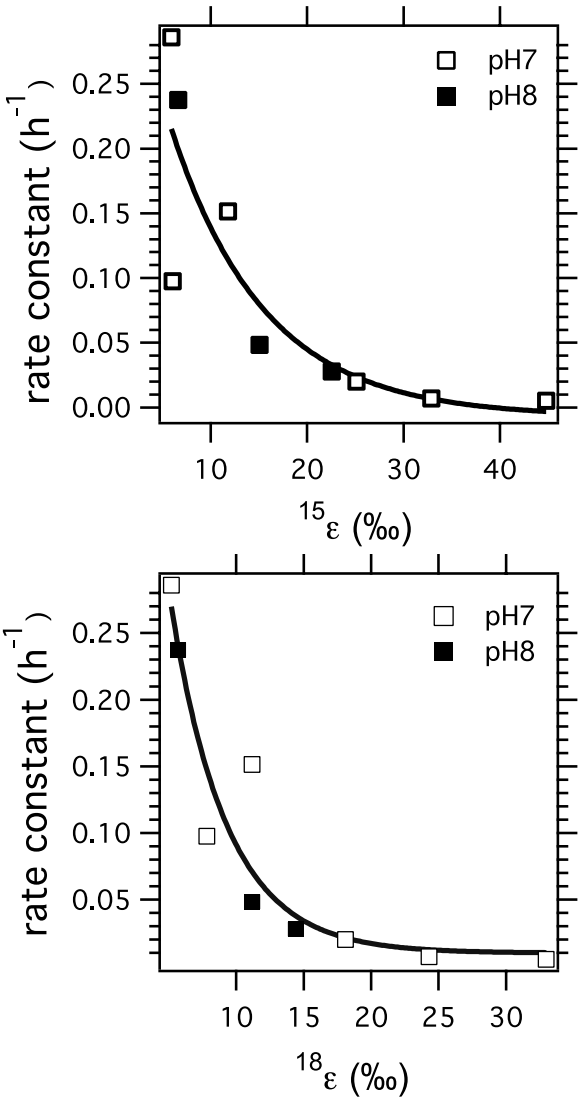

Figure 4. The relationship between kinetic isotope effect ($^{15}\varepsilon_{NIR}$ (top) and $^{18}\varepsilon_{NIR}$ (bottom)) and pseudo-first order rate constant. The empirical relationship with the best fit is an exponential fit with the following equations: $k = 0.0007 + 0.222 \cdot e^{-(^{15}\varepsilon - 5.93)/9.68}$ and $k = 0.0009 + 0.260 \cdot e^{-(^{18}\varepsilon - 5.20)/4.13}$. Changes in observed kinetic isotope effects as a function of reaction rate likely reflect complex shifts in reaction mechanisms, pathways and intermediates.

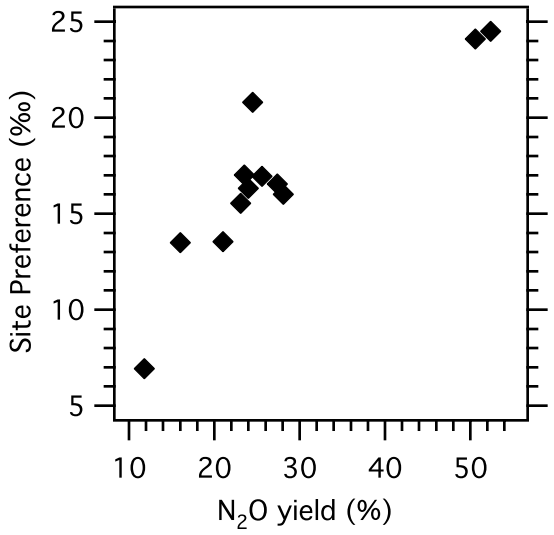

Figure 5. Site preference as related to the N_2O yield from reduction of NO_2^- by Fe(II). Changes in SP reflect differences in N_2O production mechanisms and likely reflect the formation and reactivity of nitrosyl-iron intermediates.

Supporting Information for:

Final Technical Report for DE-SC0006681

Project Title: Development of new and integrated isotope tools for characterizing nitrogen-uranium cycling in subsurface environments

PI: David Johnston

Report Title: Constraining the role of iron in environmental nitrogen transformations: Dual stable isotope systematics of abiotic NO_2^- reduction by Fe(II) and its production of N_2O

Report Authors:

Scott D. Wankel[1], Carolyn Buchwald[1], Colleen M. Hansel[1] and David Johnston[2]

1. Department of Marine Chemistry and Geochemistry, Woods Hole Oceanographic Institution, Woods Hole, MA
2. Department of Earth and Planetary Sciences, Harvard University, Cambridge, MA

METHODS

Chemical Analyses

Nitrite

Nitrite concentration was measured using the Greiss-Islovay spectrophotometric method [1]. Reactions were prepared in 1cm cuvettes in the glove box and diluted as needed with anoxic HEPES buffer. $NaNO_2$ standards of 0, 25, 50, 250 μM were run in parallel. All samples and standards received 100 μL sulfanilamide (SAN) and 100 μL naphthyl ethylene diamine (NED). Absorbance was recorded at a wavelength of 543 nm.

Fe(II)

Fe(II) concentration measurements were made using ferrozine [2]. All reactions were conducted within the glove box followed by immediate measurement on the spectrophotometer at 562 nm. Reactions were done in 1cm cuvettes with 2.7 mL of ferrozine, and 0.3 mL of sample. At higher Fe concentrations samples were diluted as necessary with anoxic HEPES buffer.

Mineral Analysis

The speciation of Fe was determined using synchrotron-based X-ray absorption spectroscopy (XAS) [3] (see Supporting Information). Samples were anaerobically mounted on a Teflon plate and sealed with Kapton polymide film to prevent moisture loss and oxidation while minimizing X-ray absorption. XAS was performed at the Stanford Synchrotron Radiation Lightsource (SSRL) on beamline 11-2 using a He-purged sample chamber. Spectra were acquired from -200 to approximately 1000 eV around the K-edge of Fe (7111 eV). The mineralogical composition of the sediments was obtained using the extended region of the XAS spectra (EXAFS region). Percentages of various Fe phases were determined by linear combination fitting (LCF) of k^3-weighted EXAFS (LC-EXAFS) spectra with a set of reference standards as described in detail previously [3] using the fitting program SIXPack [4].

References:

1. Pai, S.-C.; Yang, C.-C.; Riley, J. P., Formation kinetics of the pink azo dye in the determination of nitrite in natural waters. *Analytica Chimica Acta* **1990,** *232*, 345-349.
2. Stookey, L. L., Ferrozine - A New Spectrophotometric Reagent for Iron. *Analytical Chemistry* **1970,** *42*, (7), 779-781.
3. Hansel, C. M.; Benner, S. G.; Neiss, J.; Dohnalkova, A. C.; Kukkadapu, R. K.; Fendorf, S., Secondary mineralization pathways induced by dissimilatory iron reduction of ferrihydrite under advective flow *Geochimica et Cosmochimica Acta* **2003,** *67*, (16), 2977-2992.
4. Webb, S. M., SIXPack a graphical user interface for XAS analysis using IFEFFIT. *Physica Scripta* **2005,** *T115*.

Supplementary Figures and Tables

Table S1. Experimental conditions for each incubation.

pH	Starting $[NO_2^-]$ (μM)	Starting [Fe(II)] (mM)	Goethite added
7	200	0.5	No
7	200	4.7	No
7	200	8.4	No
8	200	0.6	No
8	200	4.2	No
8	200	6.3	No
7	200	0.8	Yes
7	200	4.8	Yes
7	200	7.9	Yes
8	200	1.0	Yes
8	200	4.5	Yes
8	200	8.9	Yes

Table S2. First-order rate constants for nitrite reduction at pH 7 and pH 8

pH	Starting [Fe(II)] (mM)	Goethite added	**k_1 (h^{-1})**	**Initial Rate ($\mu M\ h^{-1}$)**
7	0.5	No	**0.0007**	**0.1**
7	4.7	No	**0.02**	**4.0**
7	8.4	No	**0.10**	**19**
8	0.6	No	**0.03**	**5.9**
8	4.2	No	**0.23**	**41**
8	6.3	No	**0.35**	**60**
7	0.8	Yes	**0.005**	**1.0**
7	4.8	Yes	**0.15**	**28**
7	7.9	Yes	**0.29**	**50**
8	1.0	Yes	**0.05**	**9.8**
8	4.5	Yes	**0.69**	**99**
8	8.9	Yes	**1.68**	**160**

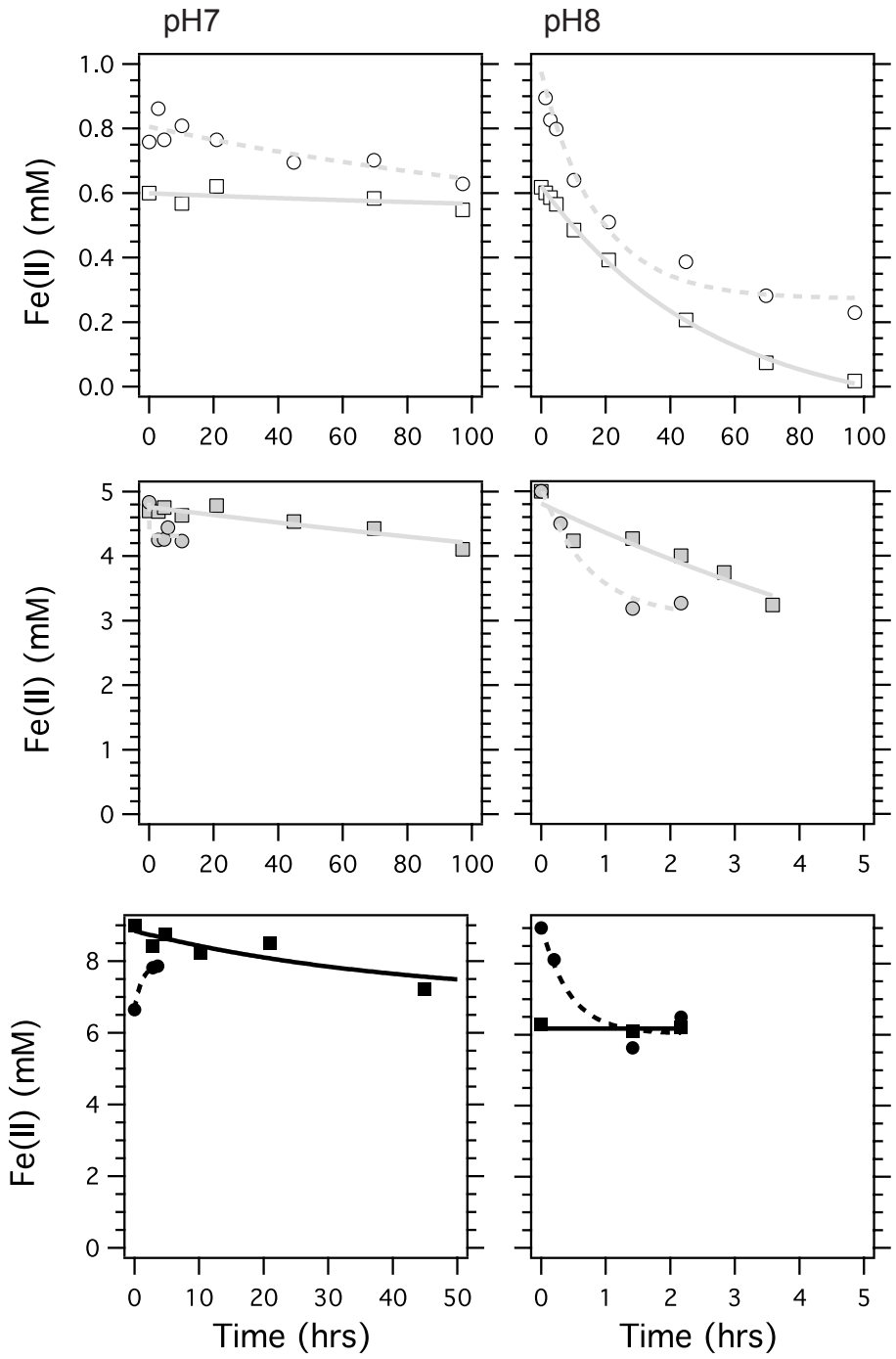

Figure S1. Dissolved Fe(II) concentration as a function of time, shown in panels by pH and Fe(II) concentration (note the time scale change at higher iron and high pH). Circles refer to experiments in which incubations were amended with goethite. A change in the aqueous Fe(II)

levels in the goethite incubation at the highest Fe(II) concentration at pH 8 was not observed, likely due to the rapid and extensive sequestration of Fe(II) within the solid phase.

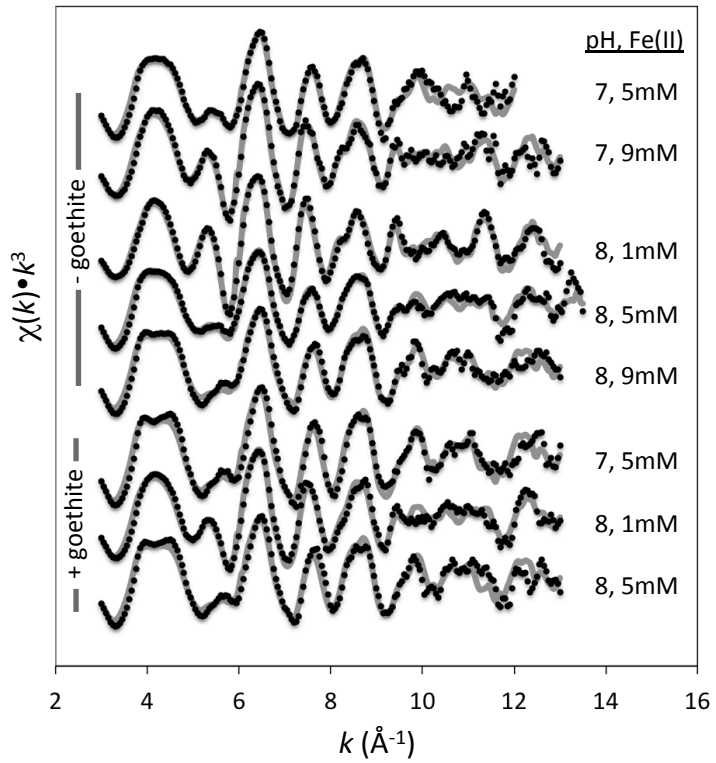

Figure S2. k^3-weighted EXAFS spectra (dotted black line) and linear combination fits (solid gray line) for the mineral percentage shown in Figure S2 obtained for incubations containing 200 μM nitrite, ferrous Fe(II) (~1, 5, or 9 mM) at pH 7 or 8 and in the presence (+) or absence (-) of goethite.

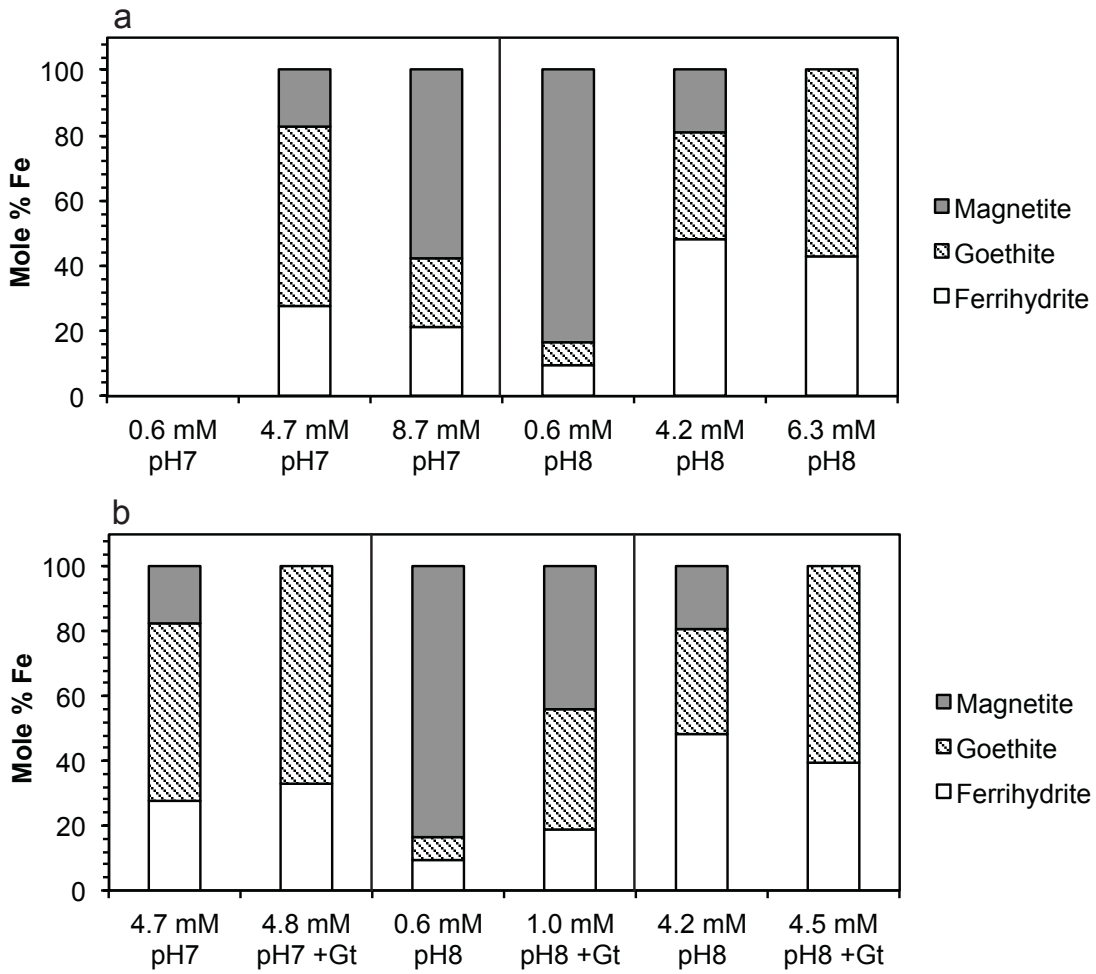

Figure S3. Summary of the final secondary minerals formed at the end of the Fe(II)-nitrite incubations. Mineral proportions were obtained via linear combination EXAFS shown in Figure S2.

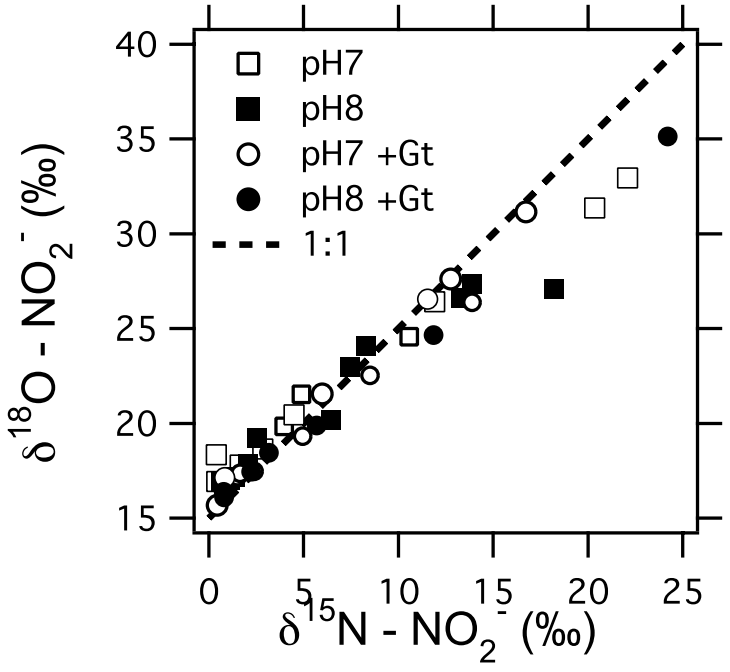

Figure S4. $\delta^{18}O\text{-}NO_2$ and $\delta^{15}N\text{-}NO_2$ in all incubations. The dotted line indicates a 1:1 relationship.

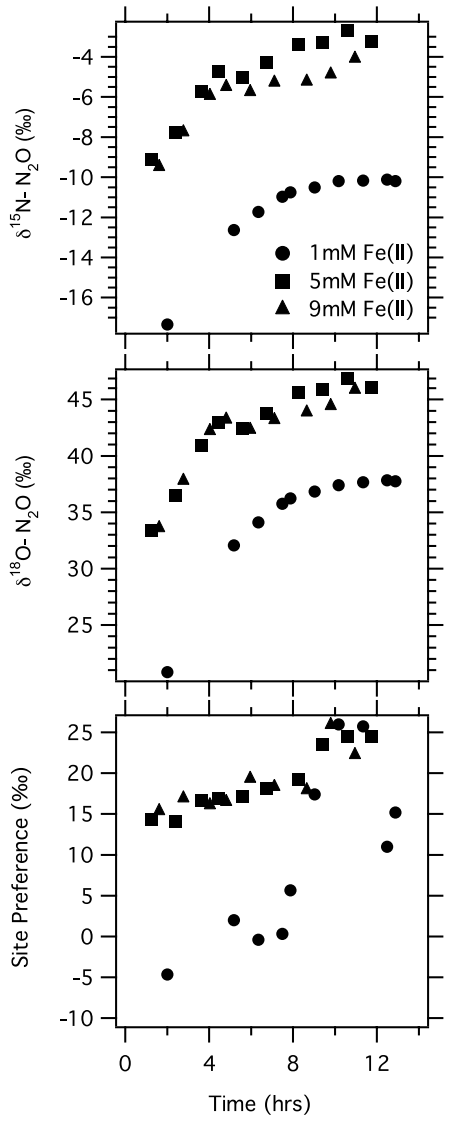

Figure S5. Time series N_2O experiments illustrating the evolution of N_2O in the sample vials over the course of the time course of the reaction. Higher Fe(II) concentrations resulted in faster reactions, higher N_2O yields (not shown) and higher $\delta^{15}N$ (top), $\delta^{18}O$ (middle) and site preference values (bottom) in comparison to reactions at ~1mM Fe(II).

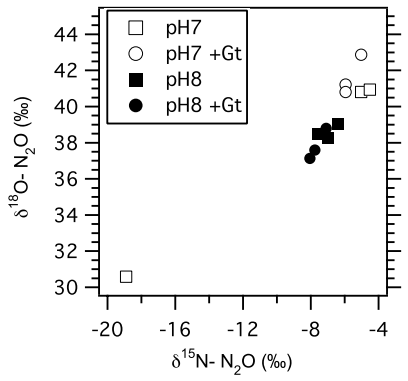

Figure S6. The dual N and O isotopic composition of N_2O produced during nitrite reduction by Fe(II). The single outlier having the lowest $\delta^{15}N$ and $\delta^{18}O$ represents N_2O produced from a partially consumed NO_2^- pool, while all others reflect N_2O produced after complete NO_2^- reduction.